Original scientific paper
https://doi.org/10.33180/InfMIDEM2021.105

Informacije MIDEM
Journal of Microelectronics,
Electronic Components and Materials
Vol. 51, No. 1(2021), 73 – 84

Effect of Dipole Position and Orientation on Light Extraction for Red OLEDs on Periodically Corrugated Substrate - FEM Simulations Study

Milan Kovačič

University of Ljubljana, Faculty of Electrical Engineering, Ljubljana, Slovenia

Abstract: One of the main efficiency-limiting factors for organic light-emitting diodes (OLEDs) is poor light extraction, which typically reaches only 20% (in best cases up to 30%) in flat standard devices. Optical modeling and simulations play an important role in improving light extraction and optimizing outcoupling efficiency. Using FEM modeling approach, the effect of dipole positions and orientations for red OLEDs on periodically corrugated substrate is evaluated and used to enhance the outcoupling efficiency. It is shown that with only 3 carefully selected dipole positions, the outcoupling efficiency over the whole area can be predicted with very reasonable accuracy, which greatly reduces the number of simulations required. The presented modelling approach is used for optimization of the sine texture as a substrate corrugation structure. OLEDs with optimized simulated texture show a relative improvement of light outcoupling from the thin film stack to the substrate by more than 25% compared to the flat plane devices.

Keywords: OLED; outcoupling; finite element method; optical modelling

Vpliv Pozicije in Orientacije Dipola na Izstop Svetlobe Rdečih OLED na Periodično Teksturiranem Substratu – FEM Simulacijska Obravnava

Izvleček: Eden izmed glavnih dejavnikov, ki omejujejo učinkovitost organskih svetlečih diod (OLED), je nizka stopnja učinkovitosti izstopa svetlobe, ki pri standardnih napravah dosega le okoli 20% (v najboljših primerih pa do 30%). Optično modeliranje in simulacije igrajo pomembno vlogo pri izboljšanju izstopa svetlobe in optimizaciji optičnega izkoristka. Z uporabo FEM modeliranja se ovrednoti učinek položaja in usmeritve dipolov za rdečo OLED na periodično teksturiranem substratu, ki se uporablja za povečanje učinkovitosti izstopa svetlobe. Pokaže se, da je mogoče s samo 3 skrbno izbranimi položaji dipola, z dobro natančnostjo napovedati učinkovitost izstopa na celotnem območju, kar močno zmanjša število zahtevanih simulacij. Predstavljeni FEM pristop se uporabi za optimizacijo sinusne teksture kot strukture teksturiranega substrata. OLED z optimizirano simulirano teksturo kažejo relativno več kot 25% izboljšanje učinkovitosti izstopa svetlobe iz tankoplastne strukture v substrat v primerjavi s ploščatimi napravami.

Ključne besede: OLED; izstop svetlobe; metoda končnih elementov; optično modeliranje

** Corresponding Author's e-mail: milan.kovacic@fe.uni-lj.si*

1 Introduction

Organic light-emitting diodes (OLEDs) have in recent years achieved a commercial widespread in display technology, especially in mobile and television displays. OLEDs are also very promising for general indoor and outdoor lighting, due to low cost, high efficiency, and high color quality. OLEDs can be fabricated as a large area sources on rigid or flexible substrates, can be made transparent for application on windows, all of which is important in lighting and architecture design [1]–[5]. OLEDs based on phosphorescent [6] and more recently on thermally activated delayed fluorescence

emitters [7], [8] have already achieved internal efficiencies close to 100%. On the other hand, highest *EQE*s for typical flat plane devices reaches only 20-30%, which is due to high optical losses resulting in poor light outcoupling efficiency [9].

Optical losses in OLEDs can be divided into three main groups. First are substrate losses due to total internal reflection (TIR) on the substrate/air interface, where light gets captured inside the thick substrate. Second are waveguide losses, that happen due to TIR at organic (transparent contact)/substrate interface, where light gets waveguided and eventually absorbed. Third part are losses due to coupling of light to surface plasmon polaritons (SPP) at organic/metallic interfaces. Minor losses are also due to parasitic absorption in layers [10]. There has been a lot of research and proposed solutions to improve the light outcoupling, see for example recent reviews [11], [12]. Especially on reducing the substrate losses, highly efficient solutions already exist, like attaching a half-sphere, different microtexturing [13]–[17] and others [18], [19]. On the other hand, solutions to waveguide and SPP losses exists, like micro-lens arrays [20], introducing scattering particles [21], corrugations [22], [23] and others [24], [25], but remain less researched and non-optimized. This is mainly because internal solutions are more challenging to fabricate and to integrate with OLED thin film stack, without having negative impact on electrical efficiency [26]. With this in mind, optical modelling and simulations play an important role in improving outcoupling efficiency, to predict optimal solutions prior to complicated fabrication process, to test only most promising ones. Simulations of light emission from thin film stacks with internal outcoupling solutions (e.g. texturization, corrugations, scattering particles) requires more advanced modelling approaches, compared to flat-plane devices.

In this paper, finite element method (FEM [27]) optical modelling is utilized to research effects of a corrugated substrate, which introduces internal textures in the OLED device structure itself. The aim is improved outcoupling of light into the substrate. In particular the focus is on investigation of different positions and orientations of emitting dipoles on outcoupling efficiency for red OLED on periodically corrugated substrate. FEM modelling approach, describing main considerations when simulating OLEDs, is explained. Presented model is used to analyze how number and position of simulated dipoles affect the simulated outcoupling accuracy. In addition, it is shown that in the analyzed cases already 3 specifically positioned dipoles in the simulation domain are sufficient to get good prediction of trends for outcoupling efficiency. Moreover, outcoupling efficiency and outcoupling trends of differently oriented dipoles for different positions on corrugated substrate are evaluated.

2 OLED Modelling

The outcoupling of light in OLEDs, which is the focus of this paper, can be presented by combined opto-electrical parameter called external quantum efficiency (*EQE*), which defines the ratio between the number of photons reaching the far field as useful light to the number of injected charge carriers. *EQE* is calculated using equation (1), where γ is electrical efficiency defined as ratio between the number of radiative recombination in emission layer and the number of injected charge carriers, $s_{\mathrm{el}}(\lambda)$ is normalized electroluminescent spectrum of emission material, $\eta_{\mathrm{out}}(\lambda)$ is outcoupling efficiency of generated light into far field and $\eta^{*}_{\mathrm{rad,e}}(\lambda)$ is effective radiative efficiency.

$$EQE = \gamma \int_{\lambda} s_{\mathrm{el}}(\lambda)\ \eta^{*}_{\mathrm{rad,e}}(\lambda)\ \eta_{\mathrm{out}}(\lambda)\ \mathrm{d}\lambda \tag{1}$$

where

$$\eta^{*}_{\mathrm{rad,e}}(\lambda) = \frac{\eta_{\mathrm{rad,e}}\ F(\lambda)}{1 - \eta_{\mathrm{rad,e}} + \eta_{\mathrm{rad,e}}\ F(\lambda)} \tag{2}$$

$\eta^{*}_{\mathrm{rad,e}}(\lambda)$ determines the ratio between radiative and non-radiative recombination. $\eta_{\mathrm{rad,e}}$ is the intrinsic radiative efficiency of the emitter and $F(\lambda)$ is the Purcell factor, defined as a ratio between total emitted light at the source location and total emitted light in infinitive homogeneous medium. Using optical simulations, also employed in this work, wavelength dependent outcoupling efficiency of generated light $\eta_{\mathrm{out}}(\lambda)$ and wavelength dependent Purcell factor $F(\lambda)$ are calculated, and with these and by using equations (1) and (2), *EQE* as a primary optical data can be calculated.

2.1 Modelling of light in thin film OLED stack

In OLEDs light is generated in the emission layer (EML) inside a thin film structure (e.g., see thin film structure used in this paper – Figure 1(a)) by electroluminescence emission of emitter material molecules. As sizes of these molecules are much smaller (few nanometers) than emission light wavelength (visible light), these can be treated as differently oriented point dipole sources [28]. The dipoles have specific predefined emission spectrum (determined by the molecule type) and angular intensity distribution and polarization of light according to the orientation in the layered system. Dipoles can in general have any arbitrarily orientation

which can be represented by three perpendicular dipole components, two horizontally (*x-y*) and one vertically (*z*) oriented according to the selected global coordinate system. In case of flat plane OLEDs, orientation of dipoles in the plane of layered system (*x-y*) plays no direct role on outcoupling efficiency itself (it can affect angular distribution of light) and is in most cases treated as isotopically oriented [29], thus only ratio between vertical and horizontal dipoles is considered. To describe general orientation of all emitting dipoles in the system, an anisotropy coefficient a is introduced, which is defined as the ratio between the vertical dipole component towards all three dipole components. Anisotropy coefficient $a = 1/3$ meaning isotropic orientation of dipoles, while $a < 1/3$ indicates preferential horizontal orientation of dipoles and $a > 1/3$, preferential orientation of vertical dipoles.

Simulation of flat plane devices can be quickly and efficiently done by decomposing the dipole emission into set of plane waves which are then transferred through the thin film stack by using transfer matrix method (TMM). In case of large external corrugations or other textures, TMM can be coupled with geometrical optics for complete device simulations [16], [17].

On the other hand, modelling and simulation of nanotextured, corrugated or by introducing other disruption in horizontal directions (e.g., scattering particles) requires more advanced approach.

For the modelling of nanostructured thin-film structure we use 3D optical simulator COMSOL Multiphysics [30], which is based on a finite element method. We choose FEM due to advantages over other methods (RCWA FDTD) due to possibility of better discretization with higher order approximation of field inside the element, fairly straightforward definition of material properties (dielectrics and metals) and boundary conditions (e.g. absorbing, symmetry), ability to handle complex 3-D geometry and especially delivery of steady-state solutions in frequency (wavelength) instead of time domain (e.g. FDTD).

Using FEM, an arbitrarily oriented dipole source can be placed anywhere inside the structure and its steady state can be simulated. As each dipole need to be treated as individual source in laterally large structure (incoherent relation between different dipoles), there is a problem how to set the boundary conditions of simulation domain to avoid coherent connections between different dipoles. This presents one of the main challenges in rigorous simulations of OLEDs, requiring special modelling approaches to be taken. For example, regular periodicity boundary conditions that significantly reduce the simulation domain to a single unit cell or less, cannot be used here, as imply coherent connections between sources in periodically repeated unit cells. One solution would be to put a single dipole source in a laterally large structure with dimensions large enough to take into account all effects taking place far away from the source with multiple simulations for each different dipole position and orientation [31]. Main drawback is the required size of the model, as propagation lengths can be very large, thus lateral sizes of at least 40 μm and more away from the source would be necessary to include majority of the effects. Such large models would require huge amount of computational power (especially limiting is the computer memory) and are thus not really feasible.

Alternative method is the usage of the so-called Floquet transform method [32], [33] (FTM). FTM highly reduces memory requirements as it enables simulations of a single period (geometry) with individual source anywhere in the basic cell by using the Floquet transform to decompose non-periodic dipole source to a linear superposition of Bloch periodic terms. Details on the method itself can be found in [32]. Drawback of this approach is that it requires large number of simulations for accurate results (many Bloch periodic terms). Numerous simulations are required due to application of different phases for in/out going waves at the edge of domain, required to cancel unwanted coherence between dipoles from neighboring domains. With parallelization this can be tolerable and FTM is also used for simulations in this work.

When constructing FEM model with FTM, we need to consider some specifics that we will describe in the following. Simulation domain needs to contain at least one, but multiple (integer) periods can also be used. On top (vertical dimension) unbounded areas that are stretching to infinity (e.g. glass, air), need to be truncated using open boundaries, absorbing all incident light with zero reflectivity. Open boundaries like perfectly matching layer (PML) or absorbing boundary conditions (ABC) are applied here. An important aspect is also the distance between open boundary and thin film stack. If the boundary is too close to the stack, possible coupling of evanescent waves to the boundary can happen influencing the simulation accuracy, on the other hand if the boundary is too far away, this can result in larger domain, requiring more computational power, elongating the simulation time. Here a rule of thumb is applied that the minimal distance between boundary and thin film stack is around 1~1.5 * simulated wavelength. In lateral directions where periodicity is applied, 2 pairs of periodic Floquet boundary conditions are used. For periodic boundary conditions, special care needs to be taken when meshing, as mesh shape and size needs to be identical on both repeating

sides, otherwise large errors can happen. For the rest of the device, meshing of the structure with general rule of thumb can be used, with 8-10 elements per distance of effective wavelength.

It needs to be mentioned that by using FTM (or other FEM method) angular intensity distribution (AID) of emitted light of OLED device in the far-field cannot be gained directly, only the total outcoupling efficiency and the Purcell factor can be calculated directly. For far field AID calculation, a reciprocity principle [34], [35] can be employed, that enables to calculate AID as a consequence of any single dipole (or continuous spatial emission by multiple dipoles) at any position in the OLED stack. For each plane wave entering from outside under specific angle of incidence, it can be recalculated (by knowing E field (simulations) at the dipole(s) location) how this dipole contributes to emission into this specific angle in the far field. Extending simulations to multiple incident angles (both zenith and azimuth), AID in the far field for all simulated incident angles can be gained. This approach can only access modes that reach the far field medium (glass, air), while all other modes are inaccessible, giving only partial data. For total evaluation, reciprocity principle for calculating AID and FTM for calculating outcoupling efficiency and Purcell factor, could be used as complementary methods, enabling simulations of device with thin and optically thick layers as well as nano and micro-sized textures or other outcoupling solutions.

2.2 Corrugated OLED structure description and model

In this contribution the focus is only on thin film stack and optical properties connected with it. In simulations glass substrate is treated as half infinitive, this is from experimental point similarly as by attaching a large glass hemisphere on top of the substrate, that enables extraction of almost all light that reaches the substrate. By this, losses due to TIR at substrate/air interface are excluded and additional back reflections into the thin film stack are neglected, thus only waveguide and SPP losses are included. Due to this, outcoupling efficiency through entire paper is considered for light reaching the substrate and consequently air by using a glass hemisphere (ignoring minimal losses at glass hemisphere/air interface). We focus on standard red bottom emitting OLED [10], [16], with high electrical efficiency $\gamma = 1$ and intrinsic radiative efficiency $\eta_{rad,e} = 0.7$. Simulated stack, with layer thicknesses marked, is presented in Figure 1(a). Emission layer (EML), where light is generated, is sandwiched between two blocking layers (for electrons - EBL and holes - HBL), and two transport layers (for electrons - ETL and holes HTL), that ensure high recombination rate in EML. Contacts are realized by opaque Ag cathode and a transparent indium tin oxide (ITO) anode. In our simulation model, EBL, HBL and EML were joined into single EML layer, to avoid very thin layers that can be very problematic to mesh and add unnecessary complexity to the device. This can be justified due to very similar optical properties of these layers so only minimal difference is expected. Emission dipoles are positioned at EML/HBL interface, as majority of recombination events occurs in vicinity of HBL, due to higher hole conductivity of EML. Entire thin film stack is deposited on top of a flat or sine textured substrate. A sinusoidal texture is selected as it is commonly used and can be experimentally fabricated on e.g. silicon or glass master by e-beam or other etching techniques. Additionally, selected sine texture exhibits smooth morphology without any abrupt changes, minimizing possibility of introducing electrical defects. All results in this contribution are related to this texture shape.

When layers are deposited on top of a textured substrate, they experience layer growth which is a combination of conformal and isotropic growth [36]. In this case a more conformal growth (linear combination of both 0.3*isotropic + 0.7*conformal) was used, which is the most common growth ratio in many amorphous materials. Actual layer growth as used in model can be seen in Figure 1(b).

a)

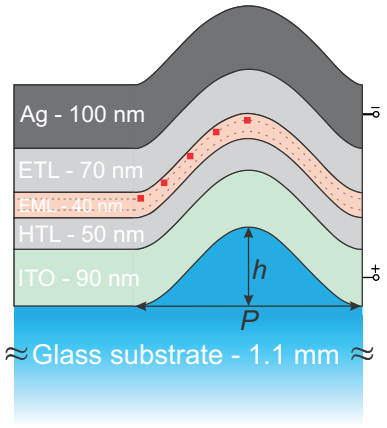

b)

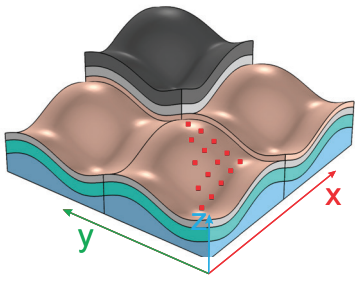

Figure 1: a.) Thin film stack of a standard red bottom emitting OLED on a corrugated glass substrate. b) Position of dipoles on a corrugated substrate (red dots shown on 1/8th of the period area only)– snapshot from Comsol simulator

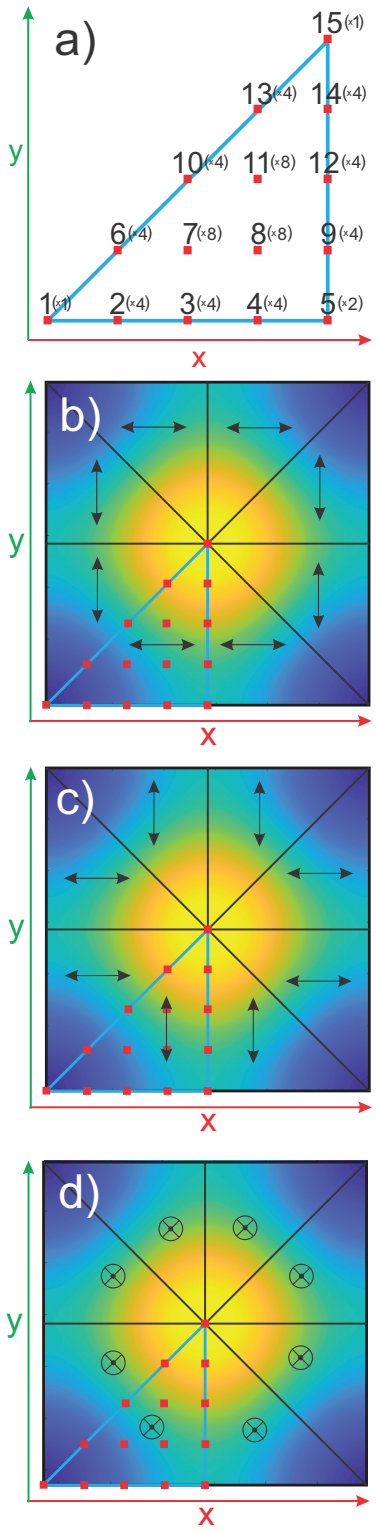

Figure 2: a.) Top view of dipole numbering on top of 1/8 of sine texture with weights factors in brackets. b-d.) Top view of sine textures, with marked dipole positions (red dots shown on 1/8th of the period area only) and arrows showing dipole orientations as defined and used in simulations. The three analyzed situations with respect to dipole orientations are denoted with horizontally – 1 (b), horizontally – 2 (c) and vertically (d) oriented dipoles.

In EML a continuous homogenous spatial emission in the emission layer is assumed, i.e. an uninterrupted distribution of dipoles across the entire emission layer. With laterally symmetrical textures, such as the 2D sine texture in this case – Figure 1 (b), an advantage of the symmetry of the structure can be taken and only dipoles on a smaller area can be simulated. In this case, this means that by considering dipoles on only 1/8 of the period (see Figure 1 (b) with red dots indicating dipole positions), the coverage of emission sources over the entire period and thus structure can be described. On the other hand, for non-symmetrical textures (e.g. saw profile or random) all possible locations of dipoles need to be considered. In the case of the sine texture, 15 dipoles positioned at constant distances from each other within the 1/8 of the texture were used, with the aim to consider as many possible positions of the dipoles on the texture, including extreme positions (e.g. on top and bottom of the texture). The numbering of the dipoles starts with no. 1 at the bottom (minimum) of the texture and ends at the top (maximum) with no. 15. Other dipole positions and corresponding number markings can be read from Figure 2(a) (top view of the dipole area, which can be linked to Figure 1(b)). It must also be taken into account that not all dipole positions, once extended to the whole period, make the same contribution to the total outcoupling efficiency, as some dipoles represent larger area than others - see Figure 2(a) (weighing factors for entire period marked with x-times) and Figure 2 (b-d). For example, area corresponding to dipole at location 15 (also 1) when extended to the whole period represent the same area as a dipole at location 7 (8 or 11) before extension, resulting in 8-times lower contribution for dipole at location 15 (or 1) than for dipole at location 7 (8 or 11). To compensate for this, an additional weighting factors are added to each simulated dipole according to the represented area in the whole structure - see weighting factors in brackets in Figure 2(a), next to the dipole number.

The orientation of the dipole is defined by its dipole moment direction, which for horizontally oriented dipoles points in the *x, y* plane and for vertically oriented dipoles in ±*z* direction according to the globally defined coordinate system and not according to the texture surface normal. For vertically oriented dipoles, this direction is uniquely defined in ±*z* direction. While for two horizontally oriented dipoles the orientation in the *x, y* plane is in general free, only with the requirement of 90 degrees between them. Due to introduced symmetry in used model, the orientation is defined in the initial simulation domain (1/8 of the period), where two horizontally oriented dipoles are differentiated as horizontally oriented - 1, where dipole moment direction points in ±*x*-direction, and as horizontally oriented - 2,

where dipole moment direction points in ±*y*-direction-see Figure 2 (b-d). Looking at the symmetry, extension over the texture diagonal leads to a change of dipole moment direction by 90 degrees in a defined coordinate system. As our definition of dipole orientation is defined on the starting 1/8 of the structure, even though the dipole moment is rotated by 90 degrees, the orientation with respect to the structure remains the same and is still treated as the same orientation as defined in the original 1/8 of the period. For details on the orientation of dipoles over the entire period, see Figure 2 (b-d).

3 Results

3.1 Flat plane device

To verify the presented FEM model, a simple device with a flat plane is simulated and results are compared (see Figure 3) with an internally developed TMM model which has been derived theoretically and verified experimentally [16].

Two orientations of dipoles are considered separately in this case: horizontally oriented-1 (identical results have been obtained for the horizontally oriented-2 in case of flat device) and vertically oriented (along *z* axis). In Figure 3(a) simulation results are presented for the outcoupling efficiency - $\eta_{out}(\lambda)$ and in Figure 3(b) the Purcell factor - $F(\lambda)$ (see definitions in Eq. 1). For both horizontally and vertically oriented dipoles very good agreement between the results can be observed, especially for the outcoupling efficiency. On the other hand, some differences in the Purcell factor can be seen, but the deviations from the correct results are small and should even decrease with texturization due to multiple random scattering events, resulting in reduced unwanted coherence between random scattering events resulting dipoles (boundary conditions).

3.2 OLED on corrugated substrate - effect of dipole location and orientation

FEM model is used to analyze optical properties, with the focus on light outcoupling of the red OLED thin-film stack deposited on a sine textured substrate with a period $P = 800$ nm and different height ranging from 0 (flat) to 400 nm (see definition of P and h in Figure 1). The effect of dipole positions and heights on outcoupling efficiency is analyzed. Results are presented for wavelength of 612 nm, that corresponds to the emission spectrum peak presented in Figure 3(a).

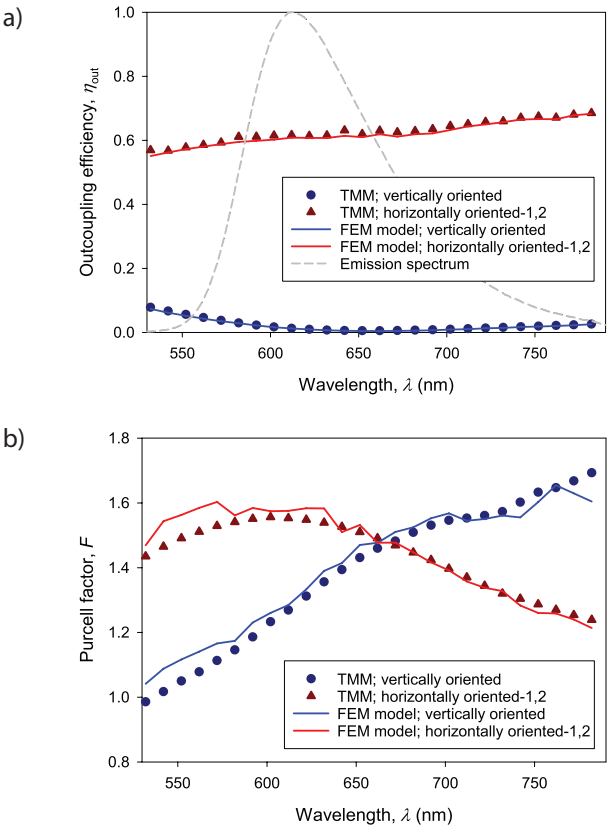

Figure 3: Comparison between two simulation models of a flat plane OLED. Symbols and lines represent results obtained with the TMM method and the FEM model, respectively. a) Outcoupling efficiency (Light extraction to substrate), b) Purcell factor.

First, the focus is on how dipole positions and orientations influence light outcoupling for different heights of the sine texture. For this, simulations of outcoupling efficiency for each of 15 dipoles individually for all three orientations and with different heights (0-400 nm) of the texture were carried out. Results of the simulations are presented in Figure 4(a-c), where lines represent outcoupling to substrate for each dipole individually and the crosses with dashed lines present weighted average of all 15 dipoles, which is actually the result corresponding to situation when all dipoles were included in calculation at once. Since the dipoles are not coupled in a coherent manner, such averaging can be carried out.

First observation from the results plotted in Figure 4 (a-c) is a high spread of results depending on the position of the dipole, indicating high influence of dipole position on the outcoupling efficiency. It has to be noted that global orientation of dipoles in one orientation set (e.g., horizontally oriented -1) remains the same independent of the dipole position. Differences are increasing with increasing texture height. This is expected, as the differences in actual vertical positions of dipoles

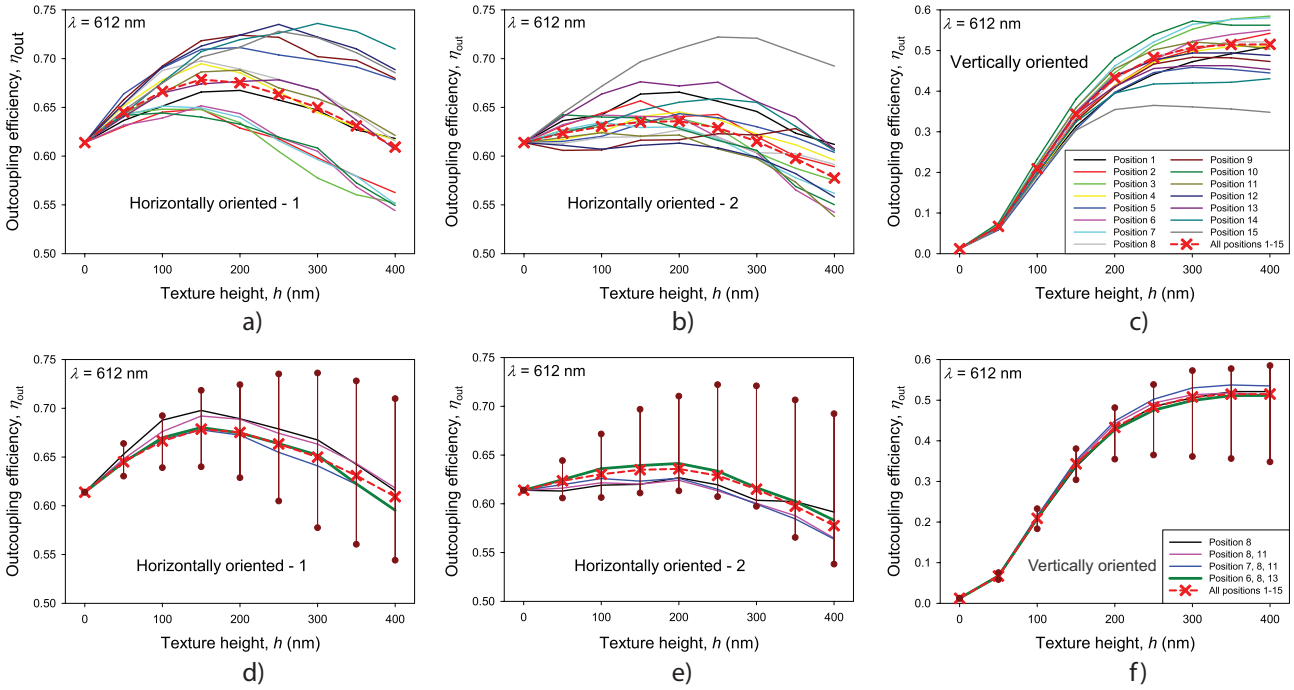

Figure 4: Outcoupling efficiency (to glass substrate) for each individual dipole according to its position on texture for different heights of the texture. a) Horizontally - 1 oriented dipoles, b) Horizontally - 2 oriented dipoles and c) Vertically oriented dipoles. d), e), f) - comparison between weighted average of all dipole positions taken into account and specifically selected ones. Added are maximum deviations for both higher and lower outcoupling efficiency. d) for horizontally - 1 oriented, e) horizontally - 2 oriented and f) vertically oriented dipoles.

are larger for the textures with higher *h*. Differences in outcoupling efficiencies between specific dipole locations can also be very high, especially for horizontal orientations, with absolute differences between minimum and maximum value above 10% for horizontal dipoles and even above 25% for vertical dipoles at texture height of 400 nm.

For a visual presentation of the effect of dipole location for the three different orientations, outcoupling efficiencies are compared again for OLED structure with the sine texture with $P = 800$, $h = 250$ (max. outcoupling with $a = 0.24$). The outcoupling efficiency according to the dipoles position on one quarter of the sine texture is shown in Figure 5. For both horizontal orientations, the highest outcoupling efficiency can be observed for the dipoles which are located on top of the texture, while outcoupling starts to decrease when moving towards the lower positions, again it slightly increases at the lower end. For horizontal-1, a high outcoupling at the ridge can be observed, while for horizontal-2 at the same position no such increase can be observed. With vertically oriented dipoles, in contrast to both horizontally oriented dipoles, a minimal outcoupling efficiency is achieved at the top end of the texture, which increases towards the middle of the texture, while outcoupling decreases again at the minimum. The outcoupling efficiency seems to follow the inclination on the texture. For horizontal dipoles a lower outcoupling at higher inclinations (separately in x or y direction for horizontal-1 and horizontal-2) is gained. While with vertical dipoles at higher inclinations a higher outcoupling efficiency is observed. This would indicate, as a highly simplified approximation, that textures with less steep features are required for an optimal outcoupling with horizontally oriented dipoles, while for vertically oriented dipoles exactly the opposite is required, i.e. textures with steeper features, indicating that the final outcoupling efficiency is a compromise between both scenarios. The optimal texture would also change with the general orientation of the dipoles, since a different texture would be optimal if there would be more vertically oriented dipoles or more horizontally oriented dipoles. Ultimately, the outcoupling cannot only be related to the inclination of the texture, as there are a number of other effects, such as the actual texture shape, the emission wavelength, the thin-film structure, all of which are specific to each individual OLED design, but these findings can serve as guidelines for further research. In addition, the mixture of many optical effects, with a high dependency not only on the shape and size of the texture but also on the emitting dipole positions and orientations, shows the importance of optical modeling and simulations for the planning, optimization and analysis of optimal optical solutions for achieving the highest outcoupling of individual OLED design.

3.3 Effect of number of dipoles used in simulations

To evaluate how much each outcoupling efficiency at each dipole position differs from weighted average, in Figure 6 total relative deviation from weighted average is presented, calculated as abs(($\eta_{out(i)}$)-$\eta_{out(average)}$) / $\eta_{out(average)}$), where *i* is the number of the dipole (1-15), and summed over all texture heights.

A high spread of deviations between all dipole positions is observed. What can also be clearly observed is the difference in the deviations at the same positions but different orientations, which indicates that the deviation is not only location-dependent but also strongly orientation-dependent. For example, dipoles at position 3 show high deviations for horizontally-1 and vertically oriented dipoles, but very low deviations for horizontally – 2 oriented dipoles. Overall, the smallest deviations for all three orientations can be observed for dipoles at position 8 and 11.

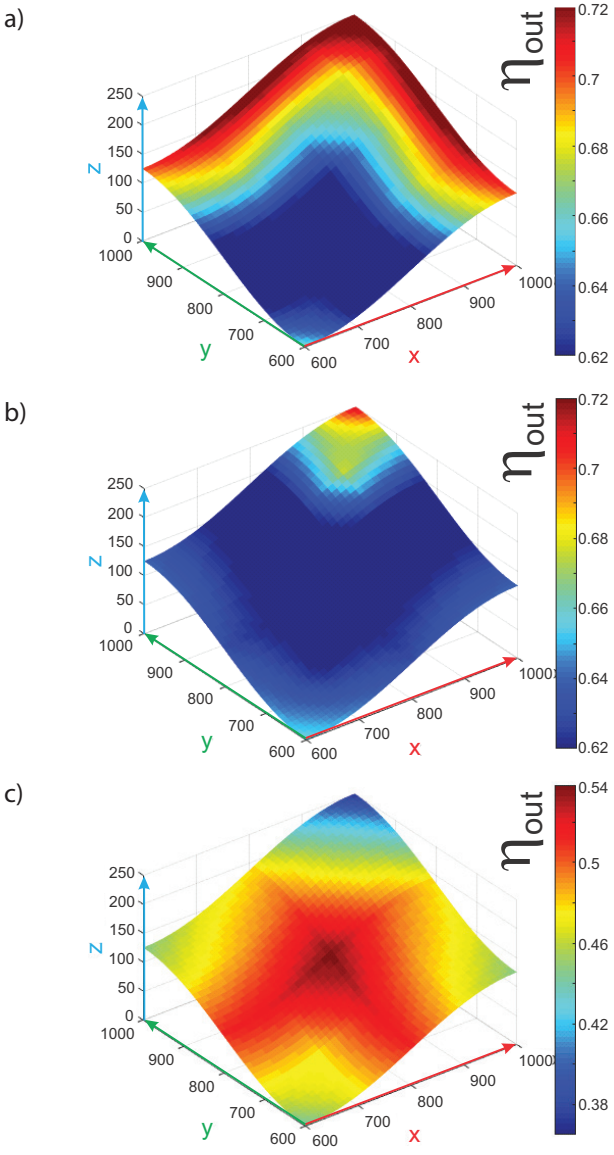

Figure 5: Outcoupling efficiency (color) for different dipole locations on top of a texture (*P* = 800, *h* = 250) for a) horizontally - 1, b) horizontally - 2 and c) vertically oriented dipoles. See Figure 2 for dipole orientation.

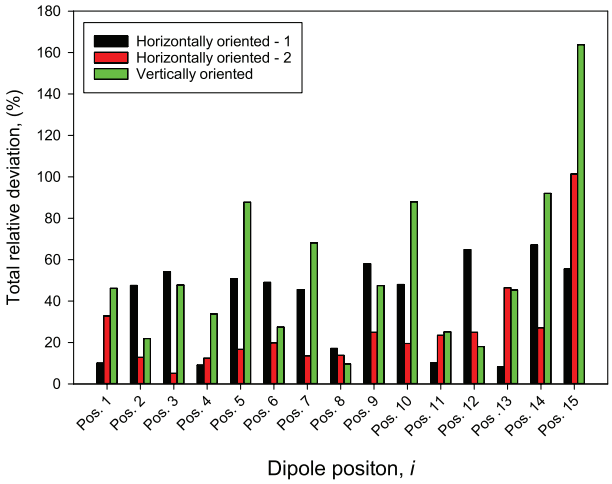

Figure 6: Total relative deviation from weighted average for each dipole and orientation.

Investigation on what is the minimal number of dipoles and what are their locations to approach the results obtained in simulations using 15 dipole locations were done. The first choice would be to take a single dipole position, preferably the dipole at position 8, which generally shows the least deviation from the averaged total data. On the other hand, a single dipole position would theoretically allow us to hit a special location where the results would differ significantly from all others (e.g., constructive or destructive coherence, etc.), so that multiple dipole positions would be preferable. To compare the outcoupling trends, in Figure 4 (d, e, f) the outcoupling for a single dipole at location 8 as the dipole with the smallest total deviation from the weighted average, the combination of the dipoles at locations 8 and 11 as two of the dipoles with the smallest deviation from the weighted average, special case of the combination of dipoles at the locations 7, 8, 11 as the combination of dipoles which are most represented on the geometry, and which are also at center locations, and at the end the combination of dipoles at the locations 6, 8, 13 which show the best agreement with the weighted average over 15 dipole locations are shown. Interestingly, the most representative combination of dipoles was the combination of dipoles at locations 6, 8 and 13, which are also located at central locations but are more widely spread than the dipoles at sites 7, 8 and 11 – see Figure 2. This combination of dipole locations follows weighted data for 15 dipole locations very well. It should be noted that even by simulating a single dipole at location 8 or a combination of other dipole locations, as shown in Figure 4 (d, e, f), a good agreement with general trends

is obtained, albeit with an over- or under- estimation of the actual outcoupling efficiency. These results show that even by simulating a smaller number of carefully selected dipole locations, it is possible to predict outcoupling trends, which greatly reduces the simulation time, although for the most accurate data, as many dipole positions as possible would have to be included in the simulations. On the other hand, it must also be mentioned that not every dipole location or even the combination of two or three dipole locations with the wrong selection (e.g. dipoles at extreme points, symmetry, e.g. no. 1, 5, 15) leads to good results. Not only can these results differ significantly from the actual data, they can also lead to false trends. In Figure 4(d, e, f), vertical lines representing the maximum and minimum output values at each texture height are added, showing high deviations from the actual weighted average, and also different trends for both horizontally oriented dipoles, with maximum output at much higher heights (250 - 300 nm) of the texture than with weighted average (150 - 200 nm). Therefore, three carefully selected dipole positions, preferably in the middle and wide spread, are necessary for a good adaptation to several dipole positions. It should be noted that this study was performed for sine shaped textures, while for other texture shapes other combinations of dipole positions may be more suitable and need to be investigated separately.

3.4 Simulation improvements of outcoupling efficiency due to substrate corrugation

So far only each individual dipole by position and orientation was evaluated, without commenting on the improvement of the outcoupling as a whole. From the presented results it can be observed that with increasing height of the texture outcoupling efficiency also increases and reaches a maximum for horizontally -1 oriented dipoles at the height of 150 nm and for horizontally - 2 oriented dipoles at 200 nm, whereas with even higher heights of the texture outcoupling starts to decrease. For vertically oriented dipoles, the outcoupling efficiency increases with increasing texture height and saturates at heights above 300 nm Thus, the optimal height depends on the actual orientation of the dipoles, with which the ratio between the individual contributions can be determined, that will influence the final output. The actual orientation of the emitter material molecules on corrugated substrates may also differ from that on flat substrates and must be determined and taken into account. The advantage of modelling, where outcoupling efficiency of light is calculated for each orientation separately, is the simple and straightforward possibility to recalculate the final outcoupling to the actual distribution of the dipole orientations without additional simulations by simply weighing each contribution. If we assume for this case that the general orientation of the dipoles does not change (a = 0.24) when deposited on corrugated substrates, the highest *EQE* ($\eta_{ele} = 1, \eta_{rad} = 0.7$) for glass substrate (or for air by using a glass hemisphere) of 47.7% at a texture height of 250 nm can be found, which is more than 25% higher than for flat plane device with 37.6% *EQE* – see Figure 7(b), indicating a high potential of sine corrugated substrates for the outcoupling of light from the OLED thin film structure. Moreover, added is outcoupling efficiency as calculated by using only 3 dipole locations (6, 8, 13), to show almost perfect matching with the simulation results for 15 locations used. In addition, the comparison of the Purcell factor between flat and textured structure (Figure 7(a)) displays only a minimal difference, indicating that texturing does not have a major impact on the microcavity in this case.

It needs to be noted, that optimal texture height of h = 250 nm for P = 800 nm, was determined for a single wavelength at emission peak of 612 nm, while if wavelengths over entire emission spectrum would be included in the optimization process, possibly different height would result in best outcoupling efficiency, thus further optimization would need to be employed.

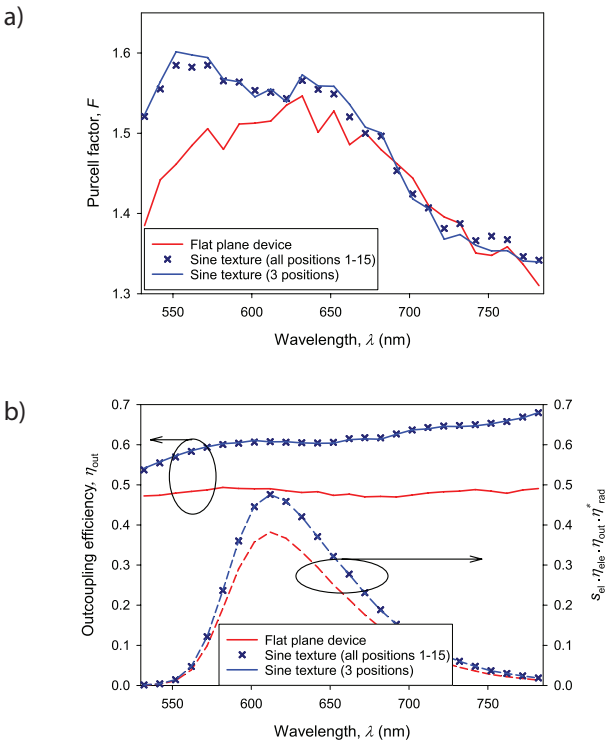

Figure 7: Comparison of simulation results for flat plane OLED and OLED on textured substrate with P = 800 and h = 250 nm. Anisotropy of a = 0.24 is considered for both cases. Added are simulations results for only 3 dipole positions (6, 8, 13). a) Purcell factor – averaged over multiple positions; b) outcoupling efficiency and *EQE* to glass substrate (to air by using a glass hemisphere)

4 Conclusions

A modeling approach based on FEM was presented to research effects of dipole position and orientation on the outcoupling efficiency of red OLED devices with periodically corrugated substrates. High deviations from the averaged outcoupling efficiency for individual positions and orientations of emitter dipoles were revealed, although it is shown that even with a smaller number (three) of carefully selected dipole positions the outcoupling over the wide area of sinusoidal texture height with very reasonable accuracy can be predicted and the number of required simulations reduced by a factor of 5. For an optimal texture, outcoupling tendencies corresponding to texture inclination are shown, with opposite effects for horizontally and vertically oriented dipoles. This shows how important it is to optimize the outcoupling solutions for each specific OLED design, especially for dipole orientation. Finally, a possible 25% improvement in *EQE* (improved outcoupling efficiency) is shown, over flat plane devices by using a sine textured substrate with a period of 800 nm and a height of 250 nm, with the possibility of additional improvements. Modeling and simulations show a high potential for further design and optimization of future outcoupling solutions.

5 Acknowledgments

The author shows appreciation to M. Topič and J. Krč for their valuable suggestions, advices and support in writing this paper. The author acknowledges the financial support from the Slovenian Research Agency (P2-0197 and J2-1727).

6 Conflict of interest

Author declares no conflict of interest.

7 References

1. Y. Chang and Z. Lu, "White Organic Light-Emitting Diodes for Solid-State Lighting," *Journal of Display Technology*, vol. 9, no. 6, pp. 459–468, Jun. 2013, https://doi.org/10.1109/JDT.2013.2248698.
2. S. Reineke, "Complementary LED technologies," *Nature Materials*, vol. 14, no. 5, Art. no. 5, May 2015, https://doi.org/10.1038/nmat4277.
3. S. Reineke, M. Thomschke, B. Lüssem, and K. Leo, "White organic light-emitting diodes: Status and perspective," *Rev. Mod. Phys.*, vol. 85, no. 3, pp. 1245–1293, Jul. 2013, https://doi.org/10.1103/RevModPhys.85.1245.
4. J. Song, H. Lee, E. G. Jeong, K. C. Choi, and S. Yoo, "Organic Light-Emitting Diodes: Pushing Toward the Limits and Beyond," *Advanced Materials*, vol. 32, no. 35, p. 1907539, 2020, doi: https://doi.org/10.1002/adma.201907539.
5. Y. Yin, M. U. Ali, W. Xie, H. Yang, and H. Meng, "Evolution of white organic light-emitting devices: from academic research to lighting and display applications," *Mater. Chem. Front.*, vol. 3, no. 6, pp. 970–1031, May 2019, https://doi.org/10.1039/C9QM00042A.
6. L. Xiao, S.-J. Su, Y. Agata, H. Lan, and J. Kido, "Nearly 100% Internal Quantum Efficiency in an Organic Blue-Light Electrophosphorescent Device Using a Weak Electron Transporting Material with a Wide Energy Gap," *Advanced Materials*, vol. 21, no. 12, pp. 1271–1274, 2009, https://doi.org/10.1002/adma.200802034.
7. D. Volz, "Review of organic light-emitting diodes with thermally activated delayed fluorescence emitters for energy-efficient sustainable light sources and displays," *JPE*, vol. 6, no. 2, p. 020901, Apr. 2016, https://doi.org/10.1117/1.JPE.6.020901.
8. Z. Yang *et al.*, "Recent advances in organic thermally activated delayed fluorescence materials," *Chem. Soc. Rev.*, vol. 46, no. 3, pp. 915–1016, Feb. 2017, https://doi.org/10.1039/C6CS00368K.
9. S. R. Forrest, D. D. C. Bradley, and M. E. Thompson, "Measuring the Efficiency of Organic Light-Emitting Devices," *Advanced Materials*, vol. 15, no. 13, pp. 1043–1048, 2003, doi: https://doi.org/10.1002/adma.200302151.
10. R. Meerheim, M. Furno, S. Hofmann, B. Lüssem, and K. Leo, "Quantification of energy loss mechanisms in organic light-emitting diodes," *Appl. Phys. Lett.*, vol. 97, no. 25, p. 253305, Dec. 2010, https://doi.org/10.1063/1.3527936.
11. M. C. Gather and S. Reineke, "Recent advances in light outcoupling from white organic light-emitting diodes," *JPE*, vol. 5, no. 1, p. 057607, May 2015, https://doi.org/10.1117/1.JPE.5.057607.
12. A. Salehi, X. Fu, D.-H. Shin, and F. So, "Recent Advances in OLED Optical Design," *Advanced Functional Materials*, vol. 29, no. 15, p. 1808803, 2019, https://doi.org/10.1002/adfm.201808803.
13. S. Möller and S. R. Forrest, "Improved light outcoupling in organic light emitting diodes employing ordered microlens arrays," *Journal of Applied*

Physics, vol. 91, no. 5, pp. 3324–3327, Feb. 2002, https://doi.org/10.1063/1.1435422.

14. H. Greiner, "Light Extraction from Organic Light Emitting Diode Substrates: Simulation and Experiment," *Jpn. J. Appl. Phys.*, vol. 46, no. 7R, p. 4125, Jul. 2007, https://doi.org/10.1143/JJAP.46.4125.
15. H. Bae, J. S. Kim, and C. Hong, "Simulation for light extraction efficiency of OLEDs with spheroidal microlenses in hexagonal array," *Optics Communications*, vol. 415, pp. 168–176, May 2018, https://doi.org/10.1016/j.optcom.2018.01.044.
16. M. Kovačič *et al.*, "Combined optical model for micro-structured organic light emitting diodes," *Informacije MIDEM*, vol. 46, no. 4, Art. no. 4, Jan. 2017.
17. M. Kovačič *et al.*, "Coupled Optical Modeling for Optimization of Organic Light-Emitting Diodes with External Outcoupling Structures," *ACS Photonics*, vol. 5, no. 2, pp. 422–430, Feb. 2018, https://doi.org/10.1021/acsphotonics.7b00874.
18. A. Gasonoo *et al.*, "Outcoupling efficiency enhancement of a bottom-emitting OLED with a visible parylene film," *Opt. Express, OE*, vol. 28, no. 18, pp. 26724–26732, Aug. 2020, https://doi.org/10.1364/OE.397789.
19. J.-H. Yen, Y.-J. Wang, C.-A. Hsieh, Y.-C. Chen, and L.-Y. Chen, "Enhanced light extraction from organic light-emitting devices through non-covalent or covalent polyimide–silica light scattering hybrid films," *J. Mater. Chem. C*, vol. 8, no. 12, pp. 4102–4111, Mar. 2020, https://doi.org/10.1039/C9TC06449D.
20. E. Wrzesniewski *et al.*, "Enhancing Light Extraction in Top-Emitting Organic Light-Emitting Devices Using Molded Transparent Polymer Microlens Arrays," *Small*, vol. 8, no. 17, pp. 2647–2651, 2012, https://doi.org/10.1002/smll.201102662.
21. H.-W. Chang *et al.*, "Nano-particle based scattering layers for optical efficiency enhancement of organic light-emitting diodes and organic solar cells," *Journal of Applied Physics*, vol. 113, no. 20, p. 204502, May 2013, https://doi.org/10.1063/1.4807000.
22. Y. Li *et al.*, "Tailor-made nanostructures bridging chaos and order for highly efficient white organic light-emitting diodes," *Nature Communications*, vol. 10, no. 1, p. 2972, Jul. 2019, https://doi.org/10.1038/s41467-019-11032-z.
23. H. Liang *et al.*, "Corrugated organic light-emitting diodes to effectively extract internal modes," *Opt. Express, OE*, vol. 27, no. 8, pp. A372–A384, Apr. 2019, https://doi.org/10.1364/OE.27.00A372.
24. Y. Sun and S. R. Forrest, "Enhanced light out-coupling of organic light-emitting devices using embedded low-index grids," *Nature Photonics*, vol. 2, no. 8, Art. no. 8, Aug. 2008, https://doi.org/10.1038/nphoton.2008.132.
25. Y. Qu, C. Coburn, D. Fan, and S. R. Forrest, "Elimination of Plasmon Losses and Enhanced Light Extraction of Top-Emitting Organic Light-Emitting Devices Using a Reflective Subelectrode Grid," *ACS Photonics*, vol. 4, no. 2, pp. 363–368, Feb. 2017, doi: 10.1021/acsphotonics.6b00847.
26. D. Riedel, T. Wehlus, T. C. G. Reusch, and C. J. Brabec, "Polymer-based scattering layers for internal light extraction from organic light emitting diodes," *Organic Electronics*, vol. 32, pp. 27–33, May 2016, https://doi.org/10.1016/j.orgel.2016.02.004.
27. J.-M. Jin, *The Finite Element Method in Electromagnetics*. John Wiley & Sons, 2015.
28. M. Furno, R. Meerheim, M. Thomschke, S. Hofmann, B. Lüssem, and K. Leo, "Outcoupling efficiency in small-molecule OLEDs: from theory to experiment," in *Light-Emitting Diodes: Materials, Devices, and Applications for Solid State Lighting XIV*, Feb. 2010, vol. 7617, p. 761716, https://doi.org/10.1117/12.840043.
29. K. A. Neyts, "Simulation of light emission from thin-film microcavities," *J. Opt. Soc. Am. A, JOSAA*, vol. 15, no. 4, pp. 962–971, Apr. 1998, https://doi.org/10.1364/JOSAA.15.000962.
30. "The COMSOL® Software Product Suite," *COMSOL Multiphysics®*. https://www.comsol.com/products (accessed Jul. 17, 2019).
31. "Simulating Plasmon Effects in Nano-Structured OLED Cathodes Using COMSOL Multiphysics® Software." https://www.comsol.com/paper/simulating-plasmon-effects-in-nano-structured-oled-cathodes-using-comsol-multiph-27012 (accessed Nov. 11, 2020).
32. L. Zschiedrich, H. J. Greiner, S. Burger, and F. Schmidt, "Numerical analysis of nanostructures for enhanced light extraction from OLEDs," in *Light-Emitting Diodes: Materials, Devices, and Applications for Solid State Lighting XVII*, Mar. 2013, vol. 8641, p. 86410B, https://doi.org/10.1117/12.2001132.
33. L. Zschiedrich, T. Blome, and H. J. Greiner, "Simulation of advanced OLED light extraction structures

with novel FEM methods," in *Organic Photonics VI*, May 2014, vol. 9137, p. 91370O, https://doi.org/10.1117/12.2054146.

34. R. J. Potton, "Reciprocity in optics," *Rep. Prog. Phys.*, vol. 67, no. 5, p. 717, Apr. 2004, https://doi.org/10.1088/0034-4885/67/5/R03.
35. S. Zhang, E. R. Martins, A. G. Diyaf, J. I. B. Wilson, G. A. Turnbull, and I. D. W. Samuel, "Calculation of the emission power distribution of microstructured OLEDs using the reciprocity theorem," *Synthetic Metals*, vol. 205, pp. 127–133, Jul. 2015, https://doi.org/10.1016/j.synthmet.2015.03.035.
36. M. Sever *et al.*, "Combined model of non-conformal layer growth for accurate optical simulation of thin-film silicon solar cells," *Solar Energy Materials and Solar Cells*, vol. 119, pp. 59–66, Dec. 2013, https://doi.org/10.1016/j.solmat.2013.05.016.

Arrived: 11.11.2020
Accepted: 16.03.2021